Reaction Kinetics, Mechanisms and Catalysis (2021) 134:759–775
https://doi.org/10.1007/s11144-021-02081-x

Effect of Sn addition on the catalytic performance of a Pd–Cu/attapulgite catalyst for room-temperature CO oxidation under moisture-rich conditions

Wanjun Zhao[1] · Xiao Li[1] · Hui Dang[1] · Ruifang Wu[1] · Yongzhao Wang[1] · Yongxiang Zhao[1]

Received: 15 July 2021 / Accepted: 28 September 2021 / Published online: 5 October 2021

Abstract

Herein, the effect of $SnCl_4$ addition on the catalytic performance of Pd–Cu/attapulgite (Pd–Cu/APT) synthesized by a deposition–precipitation method has been investigated. Compared with Pd–Cu/APT, the suitable addition of Sn has a conspicuous facilitation on the catalytic performance of Pd–Cu–Sn/APT for CO oxidation. The characterization results reveal that the incorporation of Sn gives rise to the formation of SnO_2, which conduces to produce the more $Cu_2Cl(OH)_3$ active phases and Cu^+ species in Pd–Cu–Sn/APT and establish a mutual interaction between Sn and Pd, Cu species. Accordingly, the Pd^0 species generated during CO oxidation over Pd–Cu–Sn/APT can be more easily oxidized than those over Pd–Cu/APT. Additionally, the generation of SnO_2 is prone to suppress the adsorption of water vapor on the catalyst surface, hence augmenting the water resistance of Pd–Cu–Sn/APT. Therefore, Sn-modified Pd–Cu/APT catalyst exhibits the more excellent catalytic performance for CO oxidation at room temperature under moisture-rich conditions.

Keywords Pd–Cu/attapulgite · Sn addition · CO oxidation · Room temperature

Introduction

CO, typical toxic pollutant, mostly emits from the chemical industry, fossil fuel combustion and vehicle exhaust emissions, and harms the ecological environment and human life. The catalytic oxidation of CO at room temperature has been received as the main effective method to eliminate CO [1, 2], with widespread applications in air purification, gas masks, removal of CO from exhaust streams, and purification of hydrogen for proton-membrane fuel cell [3–5].

✉ Yongzhao Wang
catalyst@sxu.edu.cn

[1] School of Chemistry and Chemical Engineering, Engineering Research Center of Ministry of Education for Fine Chemicals, Shanxi University, Taiyuan 030006, China

Up to now, the extensive catalytic systems for low-temperature CO oxidation can be found over transition metal oxide catalysts [6–8], noble metal catalysts [9–11] and supported Wacker catalysts [12–14]. Among of the transition metal oxide catalysts, the Co_3O_4 and hopcalite catalysts had received euphoric concerns owing to their high catalytic activity of CO oxidation [8, 15]. However, for these catalysts, the lack of good reaction stability and strong water resistance limited their practical application [16]. The noble metal catalysts demonstrated excellent low-temperature CO oxidation reactivity [9–11], but they possessed inescapable defects. In particular, Au based catalysts could lend to deactivation during reaction or storage due to the sensitivity to halogen-including compounds and indoor light [17].

The supported Wacker catalysts (Pd–Cu/support) have received extensive attentions owing to its autologous nature, structure and unique catalytic mechanism [18–20]. And for low-temperature CO oxidation, they have become a research hotspot due to the water resistance and anti-halide poisoning ability [21]. In addition, the influence of the support on CO catalytic oxidation performance is critical. There are a series of various supports, including activated carbon [18], molecular sieve [22], alumina [14, 23], hydroxyapatite [12] and attapulgite [13, 24], utilized for supporting metal species. The catalyst over activated carbon support has weak interaction between the active Cu species and the activated carbon support, leading to the loss of chlorine and irreversible deactivation of the catalyst during the CO oxidation reaction [19]. As to molecular sieve carrier, its inherent pores easily filled with water vapor molecules diminish the gas–liquid contact area, which decreases its catalytic stability [22]. Al_2O_3 and hydroxyapatite carrier, owing the rich surface hydroxyl groups and strong hydrophilicity, would adsorb the polar molecules—water vapor molecules in the feed gas continuously and cause the condensation of water vapor molecules on the catalyst at low temperature. The agglomeration of water vapor induces the aggregation and growth of Cu species active phase, weakens the interaction between Pd and Cu, and finally leads to irreversible deactivation of the catalyst [14]. Previous researches found that attapulgite (APT) supported $PdCl_2$–$CuCl_2$ catalysts can not only readily regulate the active phase structure of Cu species, but also improve the adaptability of the catalyst to water vapor concentrations in the feed gas [19, 21, 25]. The catalyst with natural attapulgite as carrier shows obvious advantages in practical application. Therefore, it is merely not surprising that the decrease of catalytic activity when excess moisture is present in the feed gas because of aggregation and condensation of water molecules on the catalyst active sites. To our knowledge, studies dealing with promoting their moisture tolerance of Pd–Cu/attapulgite catalyst for CO oxidation to broaden its applications are still relatively scarce.

Generally, the insertion of selected metal heteroatoms into the metal oxides can affect the textural and redox properties and facilitate the improvement of the catalytic performance [8]. In recent decades, Xu et al. [26] found that doping suitable amount of Sn can enhance obviously the water resistance of Co_3O_4 catalysts for CO oxidation, which arises from the interaction between the dispersed Sn species with Co species, as well as suppress water adsorption. Liu et al. [27] investigated that the Sn-modified hopcalite catalyst showed the more exceptional moisture resistance and catalytic activity because the addition of SnO_2 can significantly suppress the

adsorption of H_2O molecules on the surface of the catalysts. Liu et al. [28] explored that SnO_2/CeO_2 showed great CO oxidation performance owing to the strong interactions between two individual components, but the influence of water vapor was not investigated. Dong et al. [29] reported that the fine water-resistance of CuO/$Ti_xSn_{1-x}O_2$ catalysts in CO oxidation could be related to the different interactions between copper oxide species and the TiO_2–SnO_2 oxide support, that is, the formation of the Cu–O–Ti (Sn) band. Fuller et al. [30] found that Pd supported on SnO_2 displays much higher activity than that on SiO_2, and the major reason is that the synergetic effect between Pd and SnO_2 support.

The above results trigged our solicitude on elevating the activity and moisture resistance of the Wacker-type catalysts for low-temperature CO oxidation. Against the backdrop of our previous work and former findings [21, 25, 31], we take advantage of Sn as promoter to modify the Pd–Cu/APT catalyst synthesized by a deposition–precipitation method for room-temperature CO oxidation. With various characterization techniques, such as N_2-physisorption, XRD, FT-IR, H_2-TPR, CO_2-TPD and XPS, the role of Sn addition on the Pd–Cu/APT catalyst is analyzed and elucidated.

Experimental

Preparation of catalysts

The Sn-modified Pd–Cu/APT catalyst was prepared by the deposition–precipitation method. The aqueous solution mixture of $PdCl_2$ (0.02 g), $CuCl_2{\cdot}2H_2O$ (1.82 g) and $SnCl_4{\cdot}5H_2O$ (1.77 g) was dripped slowly into the APT (5 g) suspension and maintained at 70 °C in a water bath under vigorous stirring. Afterwards, 10% $NH_3{\cdot}H_2O$ aqueous solution was added dropwise into the above solution mixture until the pH reached 7. The mixture was aged for 12 h before vacuum filtering and washing with deionized water. The resulted precipitate was dried in air at 80 °C for 3 h and at 120 °C for another 3 h, then the final sample was calcined at 300 °C with a heating rate of 5 °C min^{-1} in air atmosphere for 3 h. The sample obtained was denoted as PC-0.6Sn, where Pd loading content is 0.32 wt%, Cu loading content is 11 wt%, and Sn loading content is 9.5 wt%. A series of PC–Sn catalysts with different amount of Sn were synthesized with the identical procedure, only by changing the amount of $SnCl_4{\cdot}5H_2O$. Accordingly, the catalysts were named as PC-0.3Sn and PC-0.9Sn. In addition, Pd-Cu/APT sample, denoted as PC, was prepared by the identical procedure without Sn addition for the comparison purpose.

Characterization of catalysts

N_2-physisorption analysis was measured on a Micromeritics ASAP-2020 apparatus. Sample was degassed at 150 °C for 5 h before analysis. Specific surface area (S_{BET}) was determined from the nitrogen adsorption isotherm. The average pore

diameter and pore volume were obtained by the Barrett–Joyner–Halenda (BJH) method, on the basis of the desorption branch of the isotherm.

Powder X-ray diffraction (XRD) patterns were performed to verify the species present in the catalysts. XRD patterns of the samples were recorded using a Bruker D8 Advance diffraction spectrometer with Cu K_α radiation operated at 40 kV and 40 mA with a scanning speed of 2.4° min^{-1} in the 2θ range of 5–80°.

FT-IR spectra were recorded with a Bruker Tensor 27 Fourier transform infrared spectrometer in the range of 400–4000 cm^{-1} with a resolution of 4 cm^{-1}. One milligram of each powder sample was diluted with 100 mg of vacuum-dried IR-grade KBr.

Hydrogen temperature programmed reduction (H_2-TPR) experiments were performed on a Micromeritics AutoChemII 2920 Chemisorb instrument. 30 mg of sample was loaded. 5 V% H_2/N_2 (30 mL min^{-1}) mixture was introduced and the temperature was raised from room temperature to 700 °C at a rate of 10 °C min^{-1}.

Carbon dioxide temperature programmed desorption (CO_2-TPD) experiments were carried out using the AutoChemII 2920 chemisorptions analyzer. For each experiment, 300 mg of catalyst was placed in a quartz reactor and preconditioned in flowing CO_2 (30 mL min^{-1}) for 1 h at 300 °C, followed by cooling to 50 °C in CO_2 flow. Then the sample was purged with He (30 mL min^{-1}) and heated up from 50 to 700 °C at a rate of 10 °C min^{-1}.

X-ray photoelectron spectroscopy (XPS) measurements were operated on an Escalab 250Xi spectrometer with Al Kα radiation as the excitation source. The binding energies (BE) were calibrated by the C 1s binding energy (284.8 eV).

Catalytic activity test

The catalytic activity test was according to the method reported in reference [13]: 300 mg of catalyst (40–60 mesh) was used for each test. The feed gas of 0.5 V% CO in air at a flow rate of 30 mL min^{-1} was directed through a water vapor saturator immersed in a water bath, and then flowed into the reactor. The water concentration in the feed gas was about 3.3 V%. No pretreatment was applied before catalytic activity test. The quantitative analysis of CO was performed with an on-line gas chromatograph equipped with a 3 m column packed with carbon molecular sieve, a post-column methanator and a flame ionization detector (FID). In order to enhance the sensitivity of the detection, CO and CO_2 were converted to CH_4 by the methanator at 360 °C before entering into the FID. The catalytic activity was expressed by CO conversion, which was calculated according to:

$$X(\%) = \left(CO_{inlet} - CO_{outlet}\right)/CO_{inlet} \times 100,$$

Here X is the CO conversion, CO_{inlet} represents the initial CO concentration in the inlet, and CO_{outlet} represents the CO concentration in the outlet.

Results and discussion

Catalytic performance for room-temperature CO oxidation

Fig. 1 shows the CO conversion as a function of reaction time for the catalysts investigated. It is obvious that the support (APT) performs no catalytic activity during all the reaction process. Under the same reaction conditions, the initial CO conversion of the un-modified PC catalyst is merely 84%. It is worth to noting that CO conversion begins to decrease when the reaction proceeds to 1 h and finally drops to 27% after 3 h. In comparison, PC–Sn, the self-prepared Sn-modified Wacker catalyst, exhibits complete CO conversion. Interestingly, the CO conversion of PC–Sn catalyst still remains ~ 98% after the reaction implemented 200 min, that is, showing the more excellent catalytic activity and stability in the reaction gas containing 3.3 vol.% water vapor. As can be seen, the adjunction of Sn improves the catalytic activity and the moisture resistance of Wacker catalysts (Pd–Cu/APT) for room-temperature CO oxidation.

In addition, for the purpose of elaborating the effect of Sn on the catalytic properties of PC–Sn, CO conversion versus temperature plots on the PC–Sn catalysts with different Sn contents are illustrated in Fig. 2. It is found that CO conversion of PC–Sn catalysts with the addition of different Sn doping contents possess the analogous trends. In detail, PC-0.3Sn displays the lower CO conversion compared with PC-0.6Sn and PC-0.9Sn, and the catalytic activity of PC-0.6Sn almost approach to that of PC-0.9Sn in long-term test. Therefore, PC-0.6Sn is considered as the optimal catalyst for the reason of economic rationalism, and its related textural properties were illustrated in following sections.

N_2-physisorption analysis

The N_2 adsorption–desorption isotherms of the investigated support and catalysts are given in Fig. 3. All samples demonstrate a type IV isotherm with a H3-type hysteresis loop, indicating the presence of mesoporous [32]. The H3-type hysteresis

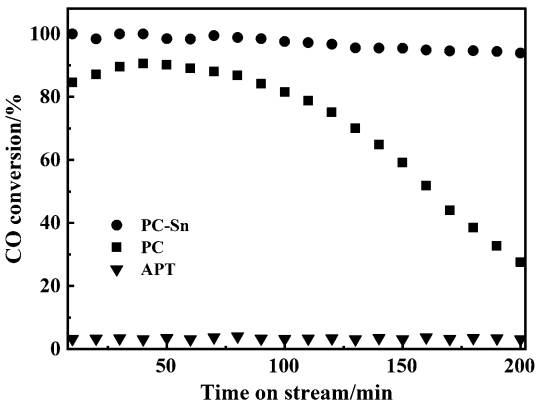

Fig. 1 Catalytic performance of APT (filled inverted triangle), PC (filled square) and PC–Sn (filled circle). Reaction conditions: 0.5% CO, GHSV 6000 h^{-1}, water vapor 3.3 V%, 25 °C

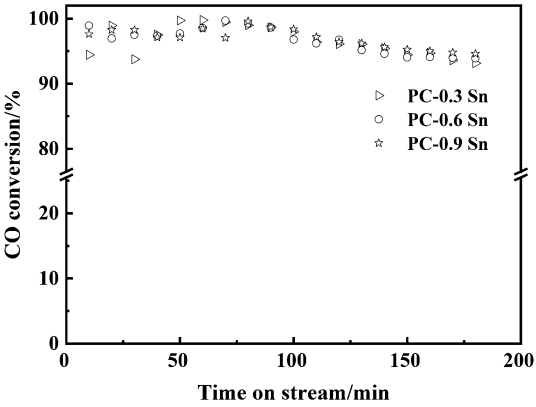

Fig. 2 Catalytic performance of PC-0.3Sn (open right facing triangle), PC-0.6Sn (open circle) and PC-0.9Sn (open star). Reaction conditions: 0.5% CO, GHSV 6000 h^{-1}, water vapor 3.3 V%, 25 °C

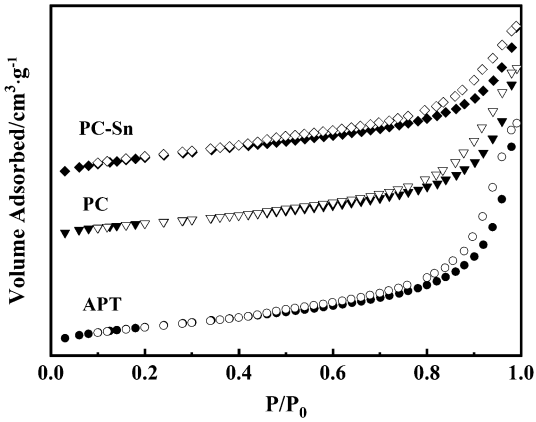

Fig. 3 N_2 adsorption–desorption isotherms of APT (Circle), PC (Inverted triangle) and PC–Sn (Rhombus). (Solid: adsorption isotherms, Hollow: desorption isotherms)

Table 1 Textural properties of APT, PC and PC–Sn

Sample	A (m^2 g^{-1})	d (nm)	V (mL g^{-1})
APT	137	10.9	0.37
PC	115	10.1	0.29
PC–Sn	158	6.81	0.27

loop manifests the materials comprised of aggregates (loose assemblages) of plate-like particles, which is the inherent nature of APT [13]. The texture properties of support and catalysts were given in Table 1. It is worth mentioning that the investigated samples show the high specific surface areas (115 ~ 158 m^2 g^{-1}) and the addition of the Sn promoter improves the texture properties of PC catalyst. Compared with APT support, the impregnation of Pd and Cu species leads to the decrease of the specific surface area of PC, which may be due to the penetration of active components into the pores of APT. At the opposite, the introduction of Sn results in the increase of the specific surface areas of PC. The pore volume and average pore

diameter diminish as the join of the Pd, Cu and Sn components, which indicates the active components and promoter probably enter into the frame of the support. It can be concluded that the specific surface area of PC–Sn expands with the participation of Sn, and the higher specific surface area of catalyst increases the contact area of active species and support, which is beneficial to the dispersion of active species.

XRD analysis

XRD measurements were performed to confirm the phase compositions of the samples calcined at 300 °C, with the patterns displayed in Fig. 4a. For the pure support (APT), the diffraction peaks at 8.5°, 13.9°, 19.8°, 20.8°, 21.5°, 23.9°, 28.8° and 35.5° are assigned to the characteristic diffraction peaks of attapulgite (JCPDS, No. 31-0783) [6]. The sharp peak at 2θ = 26.7° corresponds to the characteristic diffraction peaks of SiO_2 (JCPDS, No. 46-1045), manifesting the existence of quartz impurity in APT [33]. After loading with Pd and Cu species, the intensities of above-mentioned diffraction peaks of APT support in PC drastically decrease, indicating that Pd, Cu constituents weaken the crystallinity of the APT but preserve

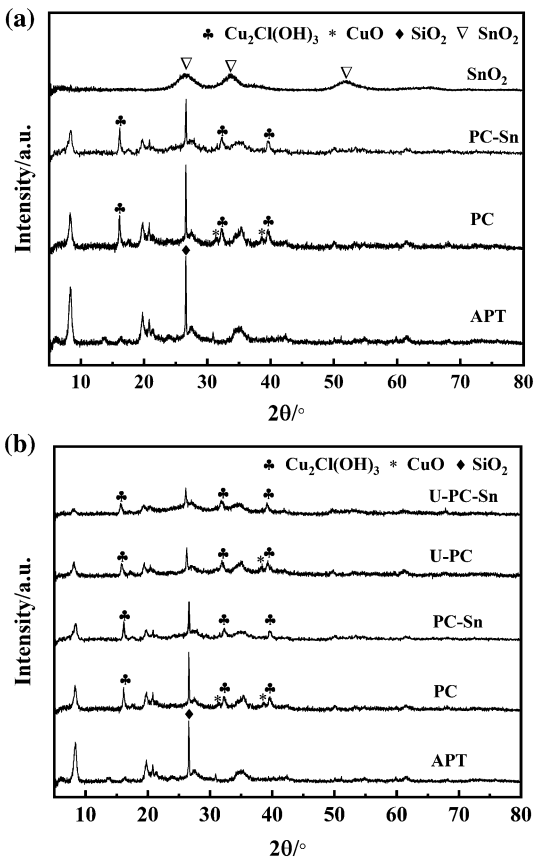

Fig. 4 **a** XRD patterns of APT, PC, PC–Sn and SnO_2. **b** XRD patterns of PC, PC–Sn after the reaction

its inherent frame structure. For SnO_2 prepared by the precipitation method, the diffraction peaks at 26.5°, 33.6°, and 52.0° are primarily attributed to the tetragonal rutile SnO_2 phase [26]. However, it is mentioned here that no any diffraction peaks related to Sn can be observed in the Sn-modified catalysts, proving that Sn species may be highly dispersed on the surface of catalysts in form of amorphous [27, 34]. Xu et al. [26] discovered that when the molar ratio of Co to Sn reached to 1.0, SnO_2 phase can be detected from the Sn-modified composite oxide catalysts. Although the loading content of Sn reaches to 9.5% in PC–Sn, the molar ratio of Cu to Sn is merely 0.47. This may provide some evidence for the absence of SnO_2 phase in PC–Sn according to the XRD results. And it is noted that the intensity of APT diffraction peaks in PC–Sn further decrease, showing that doping amorphous Sn further inhibits its crystallization. Moreover, the both catalysts display some additional nonnegligible diffraction peaks at $2\theta = 16.2°$, 32.4° and 39.6°, which are attributed to the active Cu phase in the form of $Cu_2Cl(OH)_3$ (JCPDS, No. 50-1559) for CO oxidation [23]. In addition, the characteristic diffraction peaks of CuO are detected at $2\theta = 35.5°$ and 38.7°. Interestingly, it can be found that the intensity of CuO diffraction peaks in PC–Sn is much weaker than that in PC, which may originate from the effect of $SnCl_4$ promoter. However, no characteristic diffraction peak of Pd species is observed in both catalysts, either modified or un-modified samples, owing to the low content of Pd or its high dispersion on the surface of catalysts. The XRD patterns of two samples used (U–PC–Sn, U–PC) are shown in Fig. 4b. The diffraction peaks of the $Cu_2Cl(OH)_3$ phase and APT supports can be clearly observed in the XRD pattern of U–PC–Sn, which implies that the PC–Sn catalyst possesses fine structural stability and provides strong evidence for its excellent catalytic activity and stability. And the XRD pattern of U-PC also has not changed significantly after the reaction. Hence, it can be inferred that the deactivation of the PC catalyst is not mainly caused by the change of the catalyst structure.

FT-IR analysis

In order to elucidate the effects of the Sn promoter on the catalysts, the FT-IR spectra of the samples were further characterized and are shown in Fig. 5. The bands of the support APT at 3619 and 3547 cm^{-1} originate from the stretching vibration of hydroxyl in the coordinated water and the bond water, respectively [35]. The band appears at 1654 cm^{-1} is assigned to the –OH bending vibration of all kinds of water. The broad band at 3410 cm^{-1} may be caused by the stretching vibrations of –OH in the zeolitic water or surface adsorbed water in APT [19]. And the bands emerging at 1031 and 980 cm^{-1} are associated with the Si–O–Si vibration and the in-layer Si–O bands [36]. In comparison with PC catalyst, the transmittance of the O–H peaks in PC–Sn catalyst possesses the lower signal. Concretely, the ratio of the transmittance of the band at 3619 cm^{-1} between the two catalysts and the APT support is termed to qualitatively compare the relative amount of water molecule in the two catalysts. The ratio values of PC and PC–Sn are 0.92 and 0.84 successively, which manifests that more water molecules absorb on the surface of PC catalyst. As mentioned above, the incorporation of Sn can significantly hold back the water vapor

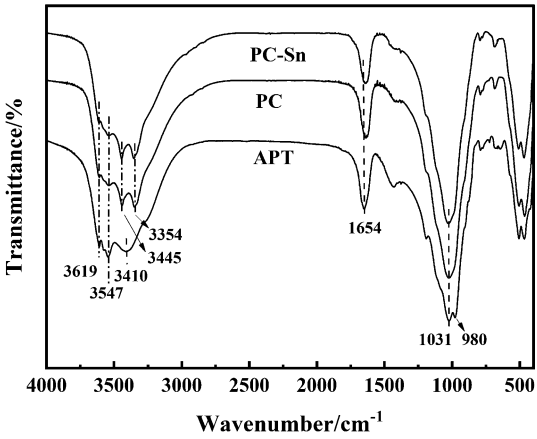

Fig. 5 FT-IR spectra of APT, PC and PC–Sn

adsorption on its surface, that is to say, it impels the enhancement of surface hydrophobicity of PC–Sn catalyst [27, 34]. Furthermore, it can be observed that the band at 3410 cm^{-1} vanishes and the two bands at 1031 and 980 cm^{-1} merge into a broad band in two prepared catalysts, probably derived from the interaction between APT and active species, leading to the surface change of the support APT [19].

Moreover, it is remarkable that the FT-IR spectra of PC and PC–Sn present two bands at 3445 and 3354 cm^{-1}, which correspond to the –OH asymmetric and symmetric stretching modes of $Cu_2Cl(OH)_3$ [37]. In order to further clarify the content of active Cu species in the catalysts, the percentage transmittance ratio of the band at 3445 cm^{-1} and 1654 cm^{-1} (T_{3445}/T_{1654}) is calculated to qualitatively determine the relative content of $Cu_2Cl(OH)_3$ species in the two catalysts. It is found that the T_{3445}/T_{1654} value of PC–Sn (2.53) is higher than that of PC (2.18). This indicates that more $Cu_2Cl(OH)_3$ species exist in PC–Sn, which is in accordance with the results of XRD. Compared with two kinds of catalysts, doping Sn facilitates the formation of more active $Cu_2Cl(OH)_3$ species, which enhances the interaction of Pd and Cu species, thereby improves the catalytic activity of PC–Sn catalyst. It is well known that the presence of water is essential for the catalytic activity of the supported Wacker catalyst, as water molecules are involved in the catalytic cycle. Nevertheless, the aggregation and condensation of excessive water vapor molecules on the catalyst active sites lead to the deactivation of the catalysts [14]. Herein, the presence of Sn suppresses effectively the absorption of water vapor on the catalyst surface, which may be the reason for the excellent catalytic stability of PC–Sn catalyst.

H_2-TPR analysis

H_2-TPR experiments were carried out to investigate the influence of Sn doping on the redox properties of concerned catalysts, with the curves of support and catalysts displayed in Fig. 6. As seen, the APT support appears no definite reduction peaks up to 400 °C, and the 2 weak broad peaks at 410 °C and 600 °C are detected, showing the reduction of a fraction of metal ions in the APT [19]. For pure SnO_2, two hydrogen

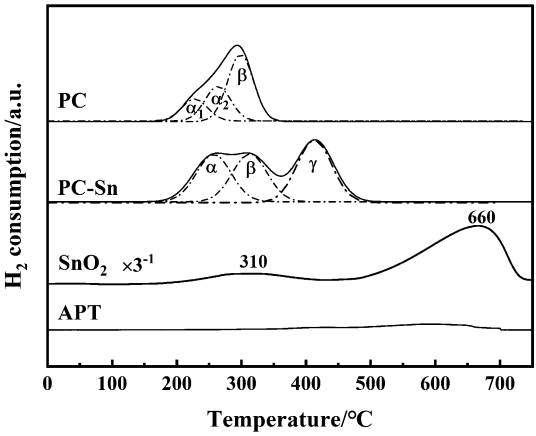

Fig. 6 TPR profiles of APT, PC, PC–Sn and SnO_2

consumption peaks at 310 °C and 660 °C can be assigned to the reduction of the surface deficient oxygen species and bulk Sn^{4+} to metallic Sn^0, respectively [34]. The reduction curve of PC catalyst emerges two types of peaks, namely, α and β. The peaks α, divided into α_1 (226 °C) and α_2 (263 °C), can be attributed to the co-reduction of microcrystalline and crystalline $Cu_2Cl(OH)_3$ with Pd species, and the peak β at 299 °C belongs to the reduction of crystal CuO [38]. Meanwhile, PC–Sn exhibits three hydrogen consumption peaks at 257, 315 and 414 °C. The peak α at 257 °C is ascribed to the co-reduction of microcrystalline $Cu_2Cl(OH)_3$ with Pd species. The peak β at 315 °C is caused by the reduction of crystal CuO. Moreover, the peak γ at 414 °C, a noteworthy big reduction peak additionally, is assigned to the reduction of partial Sn^{4+} to metallic Sn^0, proclaiming that the presence of highly dispersed SnO_2 in PC–Sn. And the reduction temperature of Sn species in PC–Sn catalyst is dramatically lower than that of the pure SnO_2, manifesting the fact that the combination or correlations of Pd, Cu and Sn species on PC–Sn. It is not difficult to find that the α and β reduction peaks of PC–Sn to shift to higher temperatures, which may be attributed to the fact that Sn enhances the interaction between Pd, Cu and APT carrier. Furthermore, the XPS results also show that there is the stronger interaction between Pd, Cu species and APT support after the addition of Sn promoter (will be presented shortly). Table 2 lists the hydrogen consumption peak parameter of catalysts. The peak area of α in PC–Sn is larger than that of PC, while the peak β for PC–Sn appears with a smaller area, revealing that the more $Cu_2Cl(OH)_3$ presents on PC–Sn than that on PC. That is to say, the role of Sn on Pd-Cu catalyst incarnates that the generation of SnO_2 in PC–Sn not only increases the amount

Table 2 Hydrogen consumption peak parameter of PC and PC–Sn

Samples	H_2 consumption (μmol g^{-1})			H_2 consumption of (α + β) (μmol g^{-1})
	Peak α	Peak β	Peak γ	
PC	510	605	–	1115
PC–Sn	575	581	758	1156

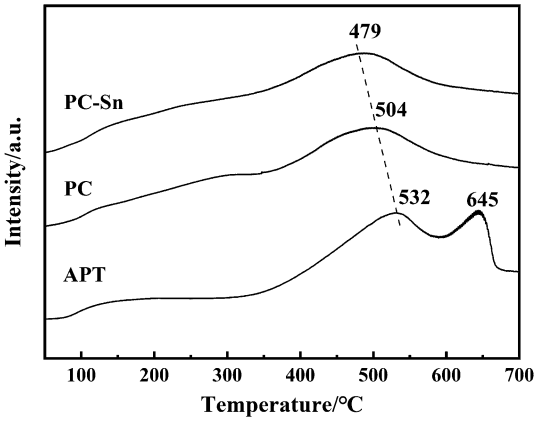

Fig. 7 CO_2-TPD profiles of APT, PC and PC–Sn

Table 3 The amounts of different basic sites of APT, PC and PC–Sn

Sample	Weak basic sites (μmol g^{-1})	Medium strength basic sites (μmol g^{-1})	Strong basic sites (μmol g^{-1})	Total basic sites (μmol g^{-1})
APT	108.6	326.5	143.5	578.6
PC	105.7	383.9	–	489.6
PC–Sn	95.5	447.9	–	543.4

of active species $Cu_2Cl(OH)_3$, corresponding to the previous XRD and FTIR results, but also enhances the synergetic interaction between Pd, Cu species and APT support.

CO_2-TPD

The support and catalysts were characterized by CO_2-TPD to detect the surface basic properties. Fig. 7 displays the CO_2-TPD profiles from 50 to 700 °C of APT, PC and PC–Sn. For APT support, there are three CO_2 desorption peaks with the increase of temperature, which are a broad CO_2 desorption peak at 100–300 °C, a stronger peak at 532 °C and a relatively sharp peak at 645 °C. The above desorption peaks at different temperatures correspond in turn to the weak, medium strength and strong basic sites in APT support. The PC and PC–Sn catalysts show similar CO_2 desorption tendency below 600 °C, and the sharp desorption peak at near 645 °C vanishes in both catalysts. The higher-temperature CO_2 desorption peaks of the two catalysts, it should be noted, divert to lower temperature, which may be insisted that the interplay between Pd-Cu components and APT support weaken the surface basic sites. Furthermore, the temperature of the CO_2 desorption peak of PC–Sn catalyst (appr. 479 °C) is lower than that of PC catalyst (appr. 504 °C). The amounts of basic sites calculated by peak areas of the support and catalysts can be seen in Table 3. It is noted that compared with PC, PC–Sn possesses the lower-temperature and the less areas of CO_2 desorption peak, which indicates that the weaker and less basic sites

present in PC–Sn. It is a common belief that the weak basic sites are more conducive to the desorption of CO_2 since the CO oxidation reaction over the catalysts occurs at room temperature [40]. Thus, it can be inferred that the relatively easy desorption behavior of CO_2 on PC–Sn can facilitate to regenerate the active sites.

XPS

Pd 3d, Cu 2p and Sn 3d XPS spectra of the catalysts are shown in Fig. 8. It can be seen from Pd 3d XPS that merely two peaks present in the PC and PC–Sn. Combined with previous work, the two peaks of Pd 3d spectra at 337.8 and 343.3 eV are assigned to Pd $3d_{5/2}$ and Pd $3d_{3/2}$, respectively [41], which states that Pd species in both catalysts only exists as Pd^{2+} [12, 24]. As shown in Fig. 8b, the Cu $2p_{3/2}$ XPS spectra of the catalysts emerge the two peaks at 934.6 and 932.3 eV, which can be ascribed to Cu^{2+} and Cu^{+} species, respectively [42]. However, it can be found that the Cu^{+} species of the PC–Sn catalyst possess the higher binding energy. This slight change of the binding energy demonstrates that the electron cloud density of Cu^{+} species decreases after the addition of the Sn promoter, which reveals the stronger interaction between Pd, Cu species and APT support. The peak areas of Cu species in PC–Sn tend to larger than those in PC with the inflow of doping Sn constituent, which reveals that the surface of PC–Sn possesses more abundant active Cu species. In addition, the binding energy of Sn $3d_{5/2}$ and Sn $3d_{3/2}$ are 486.5 and 495.0 eV, respectively (Fig. 8c), indicating a valence of + 4 for Sn ions in the PC–Sn. Corresponding to the binding energy of Sn in SnO_2 reported in literature [26], it further certificated that Sn species may exist in form of SnO_2 in the PC–Sn catalyst, which is consistent with the results of H_2-TPR. The surface compositions of catalysts are quantified and summarized in Table 4. Although the Pd valence state distributions are similar for both catalysts, the ratio of Pd^{2+} /(Cu^{+} + Cu^{2+}) in PC–Sn slightly is lower than that of PC (PC–Sn 0.146 vs. PC 0.215), showing that relatively few Pd^{2+} content in PC–Sn. It is a well-known fact that XPS is often employed to identify the surface properties of the catalysts. We conjecture that Sn species as compensation substitute for the part of surface active Pd^{2+}, which is the possible reason of the lower ratio of Pd^{2+} in PC–Sn, as evidenced by the XPS. Conversely, it is also worth explicitly noted that the ratio of Cu^{+} /(Cu^{+} + Cu^{2+}) increases to 0.324 in PC–Sn, indicating that the addition of $SnCl_4$ brings about more amount of Cu^{+} species. It is universally acknowledged that Cu^{+} is one of the active sites of Wacker catalyst for CO oxidation. Shen et al. [43] applied DRIFTS spectra combined with DFT calculation to explore the catalytic cycle of CO oxidation in the case of Pd–Cu–Cl_x/Al_2O_3 catalyst. The results indicated that Pd species is the key active sites for CO and Cu^{+} species is the active sites for O_2. Du et al. [23] found that for Cu catalysis in Wacker catalyst, O_2 was absorbed on Cu^{+} and then the O atom was transferred to Pd^{0}–CO via a redox process, resulting in CO oxidation and the formation of the positively charged Pd species. Combined with the experimental results of this work, it can be considered that the formation of SnO_2 species engenders more Cu^{+} species to participate in the reoxidation of Pd^{0} species, which is responsible for the higher CO conversion of PC–Sn in the whole reaction.

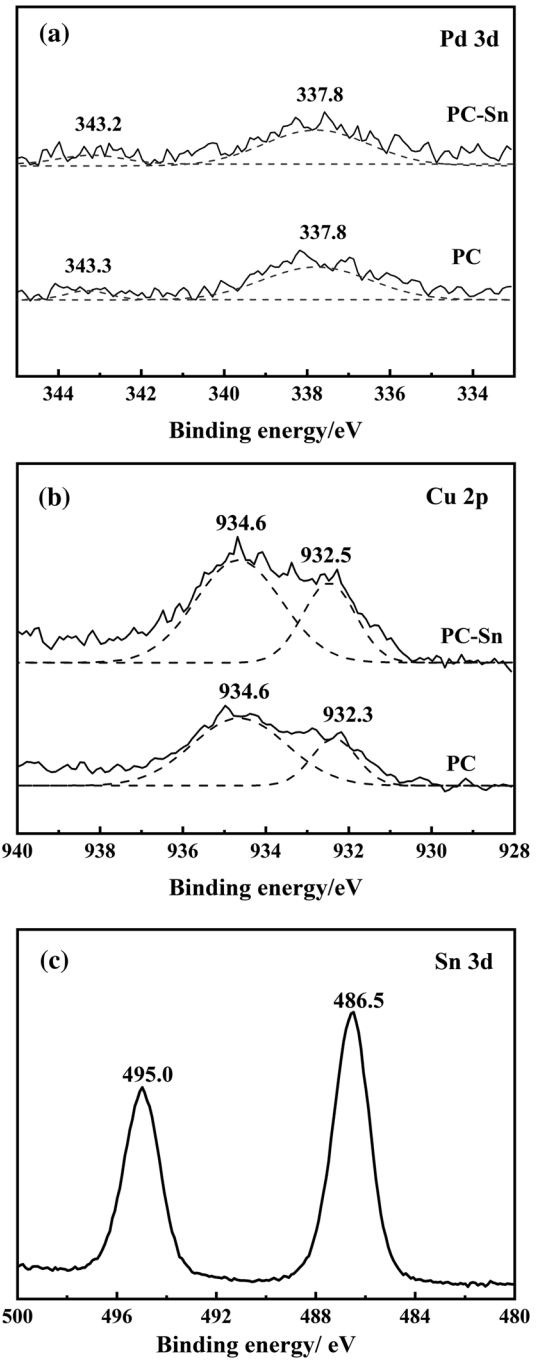

Fig. 8 **a** Pd 3d XPS spectra of PC and PC–Sn. **b** Cu $2p_{3/2}$ XPS spectra of PC and PC–Sn. **c** Sn 3d XPS spectra of PC and PC–Sn

Table 4 Parameters of PC and PC–Sn catalysts obtained from XPS analysis

Sample	Surface species ratio	
	$Pd^{2+}/(Cu^{+}+Cu^{2+})$	$Cu^{+}/(Cu^{+}+Cu^{2+})$
PC	0.221	0.250
PC–Sn	0.156	0.324

Reaction stability under the presence of water vapour is an essential issue for the catalytic activity of the supported Wacker catalyst. Water molecules can absorb and/or condensate on the active sites of most of the catalysts and deactivate the catalysts reversibly. Recently, Wang et al. [26] prepared the SnO_2-modified Co_3O_4 catalysts for CO oxidation and found that the presence of SnO_2 conduces to improve the stability and water resistance of the Co_3O_4 catalyst because the water adsorption equilibrium can be altered. In our work, after the addition of Sn, PC–Sn exhibits higher catalytic activity and better water tolerance than PC for CO oxidation in the long-term stability tests. On the basis of the XPS, H_2-TPR and FTIR results, it can be concluded that the more active Cu^{+} and highly dispersed $Cu_2Cl(OH)_3$ species present on the PC–Sn, which promotes the higher catalytic activity. The FTIR results indicate that the addition of Sn can properly reduce the amount of adsorbed water molecules on the catalyst surface, which may account for the excellent catalytic stability.

In the view of the aforementioned catalytic activity and characterization results, the PC–Sn exhibits higher catalytic activity and more excellent stability than PC for room-temperature CO oxidation under moisture-rich conditions. According to the XRD, H_2-TPR and XPS results, it can be found that compared with PC, the addition of $SnCl_4$ facilitates the formation of SnO_2 species which is highly dispersed in PC–Sn. On the basis of the XPS and FTIR results, it can be concluded that the presence of SnO_2 is prone to retain the more highly dispersed $Cu_2Cl(OH)_3$ species on the PC–Sn than PC, which interprets appropriately the higher catalytic activity on the Sn-modified catalyst. More relevantly, the SnO_2 in PC–Sn is instrumental in engendering more surface Cu^{+} species that be deemed as more active portion for catalytic cycle. And the adjunction of Sn effectively restrains H_2O adsorption on the surface of the catalysts according to the FTIR results, and it testifies that the potent water vapor resistance of the Sn-modified catalysts may account for the excellent catalytic stability. Furthermore, based on CO_2-TPD results, the weaker basic sites of PC–Sn are conducive to the desorption of CO_2, which can facilitate it to regenerate the active sites. These results can be responsible for the superior catalytic performance of Sn promoted Pd-Cu/APT catalysts for room-temperature CO oxidation under moisture-rich condition.

Based on the findings from this study, a reaction cycle for CO oxidation over PC–Sn is proposed in Fig. 9. Step 1 of the reaction mechanism depicts the adsorbed CO on active Pd^{2+} species is readily oxidized to CO_2 with the participation of water vapor molecules and concomitantly the Pd^{2+} species are reduced to Pd^{0} species. Reactivation of the catalyst is then presented in Step 2 via Pd^{0} reoxidation by neighboring Cu^{2+} in active $Cu_2(OH)_3Cl$ phases, and Cu^{2+}species could be reduced to Cu^{+}

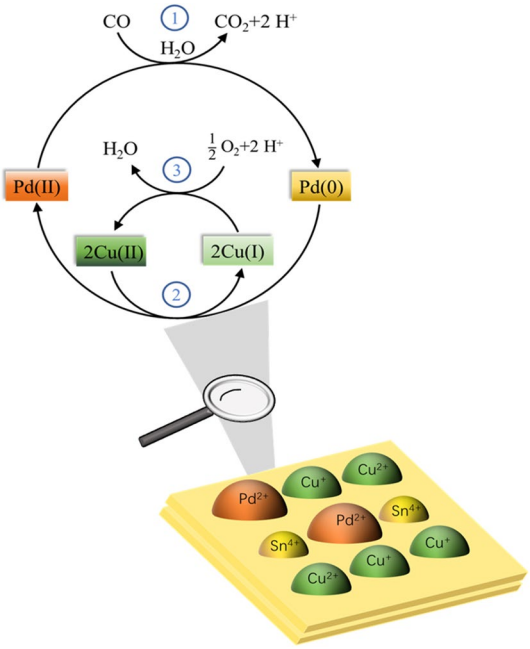

Fig. 9 A schematic mechanism of CO oxidation over PC–Sn

species. Finally, the activation of oxygen on copper is represented by Step 3 to carry out the oxidation of Cu^+ to Cu^{2+} species. As other previous reports demonstrated, the reoxidation of Pd^0 is the rate-determining step for CO oxidation [42, 43]. Thus, a large of active oxidized Cu^{2+}/Cu^+ pairs is essential in the catalytic cycle. In fact, a moderate amount of water also plays a crucial role in Wacker catalytic cycle [39, 44]. However, it cannot be ignored that when excess moisture is present in the feed gas, the aggregation and condensation of water molecules on the catalyst active sites lead to the decrease of catalytic activity [14]. In our work, the addition of Sn has a critical promoting effect on the catalytic activity and stability of the catalysts. The formation of SnO_2 in PC–Sn can not only suppress the adsorption and condensation of excess water molecules on the catalyst surface, but also is instrumental in engendering more surface Cu^+ species. Thus, PC–Sn catalyst exhibits higher catalytic performance for low temperature CO oxidation under moisture-rich condition.

Conclusions

PC and PC–Sn catalysts were prepared by the deposition–precipitation method with $NH_3{\cdot}H_2O$ as the precipitant, and the effects of $SnCl_4$ addition on the structure and catalytic performance of Pd–Cu/APT were studied. As the results of catalytic activity test, PC–Sn exhibits the superior catalytic activity and more excellent stability than PC. The reasons for better catalytic performance are derived from the formation of SnO_2 after the addition of $SnCl_4$ to Pd–Cu/APT, which conduces to the generation of more active $Cu_2Cl(OH)_3$ species, the improvement of water resistance and

the mutual interaction between Sn and Pd, Cu species. Besides, with Sn addition, the enlargement of specific surface area makes for the fine distribution of active $Cu_2Cl(OH)_3$ species in PC–Sn. And the formation of SnO_2 is instrumental in engendering more surface Cu^+ species that be deemed as more active portion for catalytic cycle, which promotes Pd^0 emerged in the reaction more easily oxidized and further contributes to remarkable catalytic performance. In conclusion, the Pd–Cu–Sn/APT could be used as an effective catalyst for low-temperature CO oxidation under moisture-rich condition, and the information given in this study may provide a new thought for researchers to refer.

Acknowledgements Authors gratefully acknowledge the financial support from Shanxi provincial key research and development plan project (Grant No. 201603D121018-1); Natural Science Foundation of Shanxi Province (Grant No. 201801D121043) and the National Natural Science Foundation of China (Grant No. 21673132).

Declarations

Conflict of interest On behalf of all authors, the corresponding author states that there is no conflict of interest.

References

1. Doggali P, Kusaba H, Einaga H et al (2011) J Hazard Mater 186:796–804
2. Zhang XD, Yang Y, Song L et al (2018) Mol Catal 447:80–89
3. Miao YX, Wang J, Li WC (2016) Chinese J Catal 37:1721–1728
4. Du N, Zhang H, Ma XY et al (2008) Chem Commun 46:6182–6184
5. Dong F, Zhao YS, Han WL et al (2017) Mol Catal 439:118–127
6. You J, Chen F, Zhao XB et al (2010) J Rare Earth 28:347–352
7. Gao JJ, Jia CM, Zhang LP et al (2016) J Catal 341:82–90
8. Wang YZ, Zhao YX, Gao CG et al (2007) Catal Lett 116:136–142
9. Gruenert W, Grossmann D, Noei H et al (2014) Angew Chem Int Edit 53:3245–3249
10. Al Soubaihi RM, Saoud KM, Myint MTZ et al (2021) Catalysts 11:131
11. Cha BJ, Kim SY, Choi CM et al (2021) Chem Eng J 404:126560
12. Li X, Xing LS, Zhao WJ et al (2020) Chem J Chinese U 41:1600–1608
13. Wang YZ, Fan LY, Shi J et al (2015) Catal Lett 145:1429–1435
14. Feng YF, Wang L, Zhang YH et al (2013) Chinese J Catal 34:923–931
15. Dey S, Dhal GC, Mohan D et al (2019) J Sci-Adv Mater Dev 4:47–56
16. Li M, Bi F, Xu Y et al (2019) Acs Catal 9:11676–11684
17. Oxford SM, Henao JD, Yang JH et al (2008) Appl Catal A-Gen 339:180–186
18. Wang SP, Li W, Dong YY et al (2015) Chinese Chem Lett 26:1359–1363
19. Wang YZ, Wang YN, Li X et al (2018) Environ Technol 39:780–786
20. Zhou FY, Du XX, Yu J et al (2016) Rsc Adv 6:66553–66563
21. Wang YZ, Cheng HM, Fan LY et al (2014) J Fuel Chem Tech 42:597–602
22. Hassan HMA, Betiha MA, Elshaarawy RFM et al (2017) Appl Surf Sci 402:99–107
23. Du X, Li HY, Yu J, Xiao X, Shi Z, Mao D, Lu G (2015) Catal Sci Technol 5:3970–3979
24. Li X, Wang YZ, Lv TT et al (2019) Catal Surv Asia 23:102–109
25. Wang YZ, Shi J, Wu RF et al (2016) Appl Clay Sci 119:126–131
26. Xu XL, Sun XF, Han H et al (2015) Appl Surf Sci 355:1254–1260
27. Liu Y, Guo Y, Peng HG et al (2016) Appl Catal A-Gen 525:204–214
28. Liu Y, Yang P, Li J et al (2015) Rsc Adv 5:98500–98507
29. Dong L, Tang Y, Li B et al (2016) Appl Catal B-Environ 180:451–462
30. Grass K, Lintz HG (1997) J Catal 172:446–452

31. Wang YZ, Fan LY, Wu RF et al (2015) J Fuel Chem Tech 43:1076–1082
32. Yuan ZY, Ren TZ, Vantomme A et al (2004) Chem Mater 16:5096–5106
33. Cao JL, Shao GS, Wang Y et al (2008) Catal Commun 9:2555–2559
34. Feng B, Shi M, Liu JX, et al (2020) J Hazard Mater 394: 122540
35. Yang HM, Tang AD, Ouyang J et al (2010) J Phys Chem B 114:2390–2398
36. Han WL, Zhang P, Pan X et al (2013) J Hazard Mater 263:299–306
37. Wei W, Gao P, Xie JM et al (2013) J Solid State Chem 204:305–313
38. Wang FG, Zhang HJ, He DN (2014) Environ Technol 35:347–354
39. Li X, Wang Y, Wei X et al (2020) Mol Catal 491:111002
40. Iriarte-Velasco U, Ayastuy JL, Boukha Z et al (2018) Renew Energy 115:641–648
41. Chlala D, Giraudon J-M, Nuns N et al (2017) ChemCatChem 9:2275–2283
42. Shen YX, Lu GZ, Guo Y et al (2011) Catal Today 175:558–567
43. Shen CL, Li HY, Yu J et al (2013) ChemCatChem 5:2813–2817
44. Harrison PG, Bailey C, Daniell W et al (1999) Chem Mater 11:3643–3654